

Stepsize sharing in time-lapse full-waveform inversion

Xin Fu*, and Kristopher A. Innanen, Dept. of Geoscience, University of Calgary, CREWES Project

Summary

Full waveform inversion (FWI) methods can produce high-resolution images of the physical properties of the subsurface. FWI has become a powerful tool for time-lapse or 4D seismic inversion, with applications in the monitoring of reservoir changes with injection and production, and potentially long-term storage of carbon. Current common time-lapse FWI strategies include the parallel strategy (PRS), the sequential strategy (SQS), the double-difference strategy (DDS). PRS time-lapse inversion is affected by convergence differences between the baseline and monitoring inversions, as well as non-repeatable noise and non-repeatable acquisition geometries between surveys. The other strategies are largely efforts to fix the sensitivities of PRS, but robust solutions are still sought. We hypothesize that several problems in time-lapse FWI arise from the independence of step lengths during updating. This is supported by synthetic data tests, which indicate that stepsize-sharing reduces artifacts caused by the variability in PRS convergence. A new strategy, we refer to as stepsize-sharing PRS (SSPRS), are then designed to address these remaining issues. The SSPRS appears to be particularly well-suited for reducing artifacts caused by convergence differences, non-repeated noise, non-repeatable source locations, and biased starting models. This breadth of robustness does not appear in any of the other approaches tested. Especially given that SSPRS through its sharing incurs half of the time cost of seeking stepsizes compared with the PRS and DDS.

Introduction

Time-lapse or 4D seismic analysis is a crucial technology for reservoir monitoring problems such as enhanced oil recovery and CO₂ storage. It has begun to be incorporated as a matter of course into reservoir development plans (Jack, 2017). Full waveform inversion (FWI) (Lailly et al., 1983; Tarantola, 1984; Virieux and Operto, 2009), a technology with the capacity to create high-resolution images of physical properties of subsurface media, has become a powerful tool for time-lapse inversion. Real field data applications have been reported with increased frequency (Raknes and Arntsen, 2014; Hicks et al., 2016; Yang et al., 2016; Kamei et al., 2017; Bortoni et al., 2021), but, as we will review next, challenges remain.

The time-lapse FWI approach we will refer to as “conventional” is known as the parallel strategy (PRS). In PRS, baseline and monitor inversions are carried out independently but using the same starting model. Its challenges derive from detailed differences within the two

independent inversions within it. They commonly exhibit different convergence properties, and these induce artifacts in the time-lapse inversion. To avoid some of these issues, Routh et al. (2012) introduced the sequential strategy (SQS), which uses the inverted baseline as the starting model for the monitor inversion. However, examples presented by Yang et al. (2015) and Zhou and Lumley (2021a) indicate that it can cause strong artifacts in the time-lapse inversion by amplifying convergence differences between the baseline and monitor inversions. Target-oriented SQS (Raknes and Arntsen, 2014; Asnaashari et al., 2015) has been shown to effectively constrain artifacts in the target zone, this mitigation strategy requires significant prior information, especially about the location of time-lapse change. Probably the most widely-adopted strategy at the moment is the double-difference strategy (DDS), proposed by Zheng et al. (2011), which has been used and adapted by many researchers (Zhang and Huang, 2013; Raknes et al., 2013; Fu and Innanen, 2021), and has been vetted with real data case in Yang et al. (2016). It has several points of weakness, some of which are addressable. For instance, Fu et al. (2020) introduced a double-wavelet DDS to mitigate the impact of non-repeatability of baseline and monitor source wavelets to the inversion. However, DDS remains very sensitive to non-repeatability of source/receiver locations (Yang et al., 2015; Zhou and Lumley, 2021b). A different approach was taken by Hicks et al. (2016), who introduced the common-model strategy (CMS) and applied it to a North Sea field case study; it was adopted by Bortoni et al. (2021) in real data of a post-salt field in the Campos Basin. A different variant, introduced by (Zhou and Lumley, 2021a) and called the central-difference strategy (CDS), has recently been shown to be robust to non-repeatable noise in time-lapse FWI (Zhou and Lumley, 2021b).

The main results of this paper is a new candidate time-lapse FWI strategy, which aim to grow and extend the robustness sought in the common strategies, and simultaneously address computational burden. The main concept we will leverage is the sharing of waveform inversion stepsizes across baseline and monitoring inversions. Conclusions are based on benchmark synthetic data and comparative inversions with the new and common methods.

Full-waveform inversion

In standard FWI (Lailly et al., 1983; Tarantola, 1984; Virieux and Operto, 2009) we minimize the L₂ norm misfit function:

$$E(\mathbf{m}) = \frac{1}{2} \|\mathbf{d}_{abs} - \mathbf{F}(\mathbf{m})\|^2, \quad (1)$$

Stepsize sharing in time-lapse full-waveform inversion

where \mathbf{d}_{obs} is the observed data or recorded wavefields, $\mathbf{F}(\cdot)$ is a forward modeling operator based on the wave equation, and \mathbf{m} is the updating model (e.g., P-wave velocity). Via some appropriate optimization approaches, based on steepest descents, conjugate gradients, etc., the model is updated iteratively as:

$$\mathbf{m}^k = \mathbf{m}^{k-1} + \delta\mathbf{m}^k, \quad (2)$$

where k is the iteration number, and

$$\delta\mathbf{m}^k = \mu^k \mathbf{g}(\mathbf{m}^{k-1}, \mathbf{d}_{res}^{k-1}), \quad (3)$$

in which

$$\mathbf{d}_{res}^{k-1} = \mathbf{d}_{obs} - \mathbf{F}(\mathbf{m}^{k-1}), \quad (4)$$

is the updating direction of model in iteration k , which depends on the updated model \mathbf{m}^{k-1} and data residual \mathbf{d}_{res}^{k-1}

in iteration $k-1$. In the steepest descent method, \mathbf{g} represents the gradient of the misfit function (equation 1) with respect to \mathbf{m} , which is the zero-lag cross-correlation between forward wavefields and backward wavefields of data residuals. For the first iteration, a starting model \mathbf{m}^0 have to be prepared, which can be obtained by velocity analysis or tomography. Furthermore, combining equation 3 and 4, we have

$$\delta\mathbf{m}^k = \mu^k \mathbf{g}(\mathbf{m}^{k-1}, \mathbf{d}_{obs}), \quad (5)$$

where the updating direction \mathbf{g} depends on observed data \mathbf{d}_{obs} and the updated model \mathbf{m}^{k-1} in iteration $k-1$. In this study, we use a time-domain constant-density acoustic finite-difference method as the forward modeling operator, the steepest descent method as the optimization, and we precondition the gradient with the diagonal approximation of the Hessian matrix (Shin et al., 2001).

Common time-lapse inversion strategies

The parallel strategy (PRS) follows the workflow in Figure 1a. It includes two independent FWI processes: baseline model inversion, with baseline data and a starting model as inputs, and monitor model inversion, with monitor data and the same (baseline) starting model as inputs. The estimated time-lapse model is the difference between the inverted monitor model and the inverted baseline model. Since FWI is highly non-linear, with local minima as common traps, the two FWI processes mentioned above often have different convergence properties, with each difference tending to produce artifacts upon subtraction.

The sequential strategy (SQS) is summarized in the workflow in Figure 1b. It involves having the same baseline inversion as PRS, and takes baseline data and a starting model as inputs. The monitor inversion is different. In it, the inverted baseline model is used as the starting model for the monitor inversion, and the difference of the two final

inversions is the time-lapse model. Inversions with different starting models also tend to produce different convergence histories, however, and again strong artifacts are the result (Yang et al., 2015; Fu et al., 2020). We do not pursue SQS further in this study.

The double-difference strategy (DDS), with workflow illustrated in Figure 1c, also contains two FWI steps. The first is again the baseline model inversion. In the second, the starting model is the inverted baseline model, as with SQS, but the input monitor data are not the observed monitor data. Instead, a composited data set is introduced:

$$\mathbf{d}_{DD} = \mathbf{F}(\mathbf{m}_{bas}) + (\mathbf{d}_{mon} - \mathbf{d}_{bas}), \quad (6)$$

where $\mathbf{F}(\mathbf{m}_{bas})$ are synthetic data predicted from the inverted baseline model \mathbf{m}_{bas} , $\mathbf{d}_{mon} - \mathbf{d}_{bas}$ are difference data (observed monitor data \mathbf{d}_{mon} minus the observed baseline data \mathbf{d}_{bas}). DDS can reduce convergence differences between baseline and monitor inversions, tending to suppress artifacts outside of the time-lapse change zone. It is, in other words, a kind of target-oriented strategy. Its disadvantages arise largely in difference data in equation 6, which are often weak. The signal is easy influenced by non-repeatability in time-lapse surveys, and those differences can leak strongly into the time-lapse model.

Stepsize sharing time-lapse inversion strategy

In this section, we propose a new strategy for time-lapse FWI that add to these mitigating efforts the idea of sharing of stepsizes. Returning to the sequence in equations 2 to 5, if we substitute equation 5 into 2, we produce an expression for an updated monitor model at:

$$\begin{aligned} \mathbf{m}_{mon} &= \mathbf{m}_{mon}^0 + \sum_{k=1}^n \mu_{mon}^k \mathbf{g}(\mathbf{m}_{mon}^{k-1}, \mathbf{d}_{mon,obs}) \\ &= \mathbf{m}_{mon}^0 + \sum_{k=1}^n \mu_{mon}^k \mathbf{g}(\mathbf{m}_{mon,bas}^{k-1} + \mathbf{m}_{il}^{k-1}, \mathbf{d}_{bas,obs} + \mathbf{d}_{dif}) \end{aligned} \quad (7)$$

where n is the maximum iteration number, μ_{mon}^k is the stepsize for iteration k during the monitor inversion, \mathbf{m}_{mon}^0 is the starting model, $\mathbf{d}_{mon,obs}$ is observed monitor data including the data ($\mathbf{d}_{bas,obs}$) corresponding to baseline model and the data (\mathbf{d}_{dif}) corresponding to the time-lapse model, and \mathbf{m}_{mon} is the inverted monitor model including the implicit baseline model $\mathbf{m}_{mon,bas}$ and time-lapse model \mathbf{m}_{il} . And the gradient \mathbf{g} which is linear with respect to the observed data and nonlinear with respect to the model can be expended via Taylor expansion as:

Stepsize sharing in time-lapse full-waveform inversion

$$\begin{aligned}
 & \mathbf{g}(\mathbf{m}_{mon,bas}^{k-1} + \mathbf{m}_{tl}^{k-1}, \mathbf{d}_{bas,obs} + \mathbf{d}_{dif}) \\
 &= \mathbf{g}(\mathbf{m}_{mon,bas}^{k-1} + \mathbf{m}_{tl}^{k-1}, \mathbf{d}_{bas,obs}) + \mathbf{g}(\mathbf{m}_{mon,bas}^{k-1} + \mathbf{m}_{tl}^{k-1}, \mathbf{d}_{dif}) \\
 &= \mathbf{g}(\mathbf{m}_{mon,bas}^{k-1}, \mathbf{d}_{bas,obs}) + \mathbf{g}'(\mathbf{m}_{mon,bas}^{k-1}, \mathbf{d}_{bas,obs}) \mathbf{m}_{tl}^{k-1} + \mathbf{g}(\mathbf{m}_{mon,bas}^{k-1} + \mathbf{m}_{tl}^{k-1}, \mathbf{d}_{dif})
 \end{aligned} \tag{8}$$

Putting equation 8 into equation 7, we have:

$$\begin{aligned}
 \mathbf{m}_{mon} &= \mathbf{m}_{mon}^0 + \sum_{k=1}^n \mu_{mon}^k \mathbf{g}(\mathbf{m}_{mon,bas}^{k-1}, \mathbf{d}_{bas,obs}) \\
 &+ \sum_{k=1}^n \mu_{mon}^k \mathbf{g}'(\mathbf{m}_{mon,bas}^{k-1}, \mathbf{d}_{bas,obs}) \mathbf{m}_{tl}^{k-1}, \\
 &+ \sum_{k=1}^n \mu_{mon}^k \mathbf{g}(\mathbf{m}_{mon,bas}^{k-1} + \mathbf{m}_{tl}^{k-1}, \mathbf{d}_{dif})
 \end{aligned} \tag{9}$$

from which the implicit baseline model can be abstracted as:

$$\mathbf{m}_{mon,bas} = \mathbf{m}_{mon}^0 + \sum_{k=1}^n \mu_{mon}^k \mathbf{g}(\mathbf{m}_{mon,bas}^{k-1}, \mathbf{d}_{bas,obs}), \tag{10}$$

where should be eliminated from the inverted monitor model to obtain the time-lapse model.

In PRS, two FWI procedures are enacted, starting from the same model, and having the same iteration number. The implicit baseline model cannot be eliminated completely in the PRS, since the stepsizes in baseline and monitor inversions are different. The remaining baseline model can be considered the source of the coherent artifacts in the final time-lapse model.

PRS can be adapted to produce the stepsize-sharing parallel strategy (SSPRS), in which the implicit baseline model is eliminated. The workflow is illustrated in Figure 2. In SSPRS, we perform the monitor inversion first with the inputs of a starting model and observed monitor data, and the outputs are not only the monitor model but also the stepsizes for each iteration. Then, in the second FWI, the baseline inversion, the inputs are not only the observed baseline data and the same starting model, but also the stepsizes from the first monitor inversion. The final time-lapse model is obtained by subtracting the baseline model from the monitor model. In addition to the elimination of what is largely a source of artifacts, an advantage of this SSPRS approach is that it saves on the cost of seeking the stepsizes during the second FWI. This is the first of the two proposed methods.

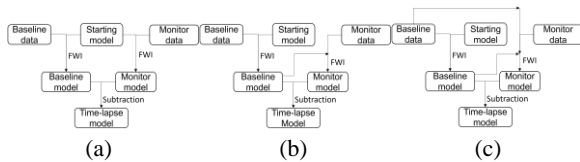


Figure 1: Workflows of (a) the parallel strategy (PRS), (b) the sequential strategy (SQS), and (c) the double-difference strategy (DDS).

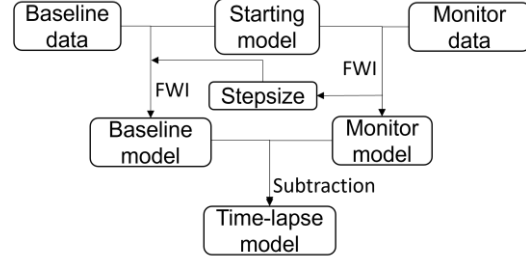


Figure 2: Workflow of the stepsize-sharing parallel strategy (SSPRS).

Numerical examples

In this section, we use a land model to test our method and have comparisons with common methods. The true baseline model is displayed in Figure 3a, two reservoirs are located at the left below corner and near the center, respectively. To mimic the fluid change, 4% or 49m/s velocity changes, displayed in Figure 3b, are added at the two reservoirs to obtain the monitor model. A starting model directly smoothed from the true baseline model is displayed in Figure 3c, which is employed in the first FWI of all time-lapse strategies mentioned above. The model size is 101-by-208 with 10m spacing. On the top of the model, seven sources are evenly spread at the depth of 10m, and each surface cell grid is located a receiver. The source wavelet used for baseline and monitor data sets is identical, which is a minimum phase wavelet with a dominant frequency of 10Hz. Next, we will implement the PRS, SSPRS, DDS to acoustic and synthetic data, and all inversions have the same iteration number.

In Figure 4, inverted time-lapse models from the PRS, SSPRS, and DDS, using noise-free data, perfectly repeatable acquisition, and unbiased starting model (Figure 3c), are plotted. We observe the time-lapse changes can be clearly seen in all results, but strong artifacts caused by the convergence difference between baseline and monitor inversions appear in the result of PRS, and the DDS and SSPRS can effectively depress the artifacts. However, in Figure 5, the DDS fails in the case of unrepeatable acquisition geometries, in which the source locations for monitor data are 20 meters larger than that for baseline data. And the PRS and SSPRS are still of good performances.

For the results in Figures 4 and 5, Starting models adopted for the first FWI are both the unbiased model in Figure 3c. Different from that, in Figures 6 and 7, we employ two biased starting models. The one for Figure 6 is that in Figure 1b plus 100 m/s, and the one for Figure 7 is that in Figure 1b minus 100 m/s. Moreover, we add 5% percent noise to the synthetic data, and the source locations for monitor data are still 20 meters larger than that for baseline data. From the

Stepsize sharing in time-lapse full-waveform inversion

results in Figure 6 and 7 we observe time-lapse changes can only be discerned in results from the SSPRS.

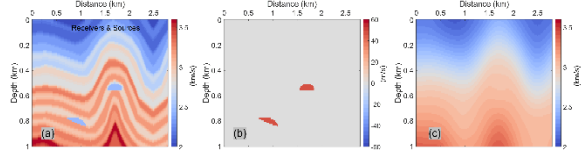


Figure 3: (a) True baseline model. (b) True time-lapse model. (c) The unbiased starting model directly smoothed from the true baseline model in Figure 3a.

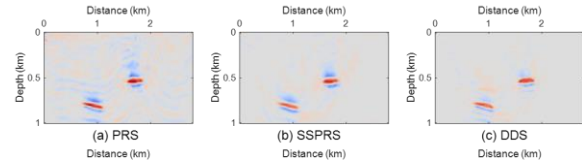


Figure 4: Inverted time-lapse models from the PRS, SSPRS, and DDS using noise-free data, perfectly repeatable acquisition geometries, and unbiased starting model in Figure 3c. All figures are clipped in the same color bar that in Figure 3b.

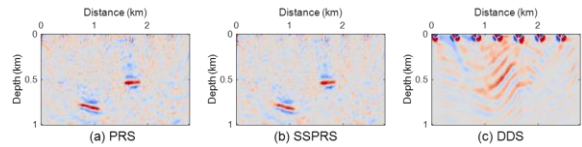


Figure 5: Inverted time-lapse models from the PRS, SSPRS, and DDS using noise-free data, unrepeatable acquisition geometries, and unbiased starting model in Figure 3c. All figures are clipped in the same color bar that in Figure 3b.

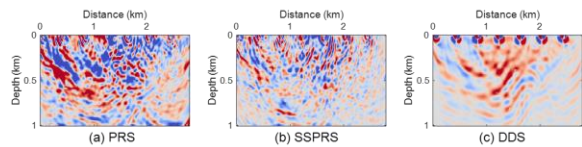


Figure 6: Inverted time-lapse models from the PRS, SSPRS, and DDS using noisy data, unrepeatable acquisition geometries, and biased starting model (unbiased starting model in Figure 3c plus 100 m/s). All figures are clipped in the same color bar that in Figure 3b.

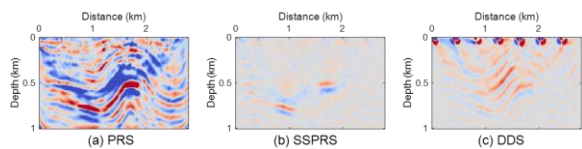


Figure 7: Inverted time-lapse models from the PRS, SSPRS, and DDS using noisy data, unrepeatable acquisition geometries, and biased starting model (unbiased starting model in Figure 3c minus 100 m/s). All figures are clipped in the same color bar that in Figure 3b.

Conclusions

We have proposed a new strategy, the SSPRS, for time-lapse FWI, and an acoustic land model has been adopted to demonstrate its feasibility and effectivity. The SSPRS keeps the frame of PRS and includes twice FWIs starting from the same model. In the SSPRS, the first FWI, which can be either the baseline inversion or the monitor inversion, outputs not only the inverted model but also the stepsizes of each iteration that are shared to the second inversion. The synthetic data tests demonstrate the SSPRS as a strategy produces results that are robust to convergence differences; the SSPRS in addition is insensitive to non-repeatable source locations and biased starting models. Not inconsequentially, the SSPRS also costs roughly half of the computation time of PRS and DDS.

Acknowledgments

We thank the sponsors of CREWES for continued support. This work was funded by CREWES industrial sponsors and NSERC (Natural Science and Engineering Research Council of Canada) through the grant CRDPJ 543578-19. Partial funding also came from the Canada First Research Excellence Fund.